Supplementary materials

Compressed Sensorimotor-to-Transmodal Hierarchical Organization in Schizophrenia

Supplementary methods

Participants

One hundred and two patients with schizophrenia were recruited from the Clinical Hospital of Chengdu Brain Science Institute; 126 HC were recruited from the local community through advertisements and word of mouth. Patients were diagnosed with schizophrenia according to the structured clinical interview for DSM-IV Axis I disorders - clinical version (SCID-I-CV). All patients received treatment with antipsychotics and did not participate in other therapy programs. Exclusion criteria included co-morbid Axis I diagnosis, active substance use disorders, or history of brain injury. HC were excluded based on current or past Axis I disorder as verified using the Structured Clinical Interview for DSM-IV, history of neurological illness, traumatic brain injury, substance-related disorders, or first-degree relatives with a history of psychosis. Two HC with poor quality of imaging data as assessed by visual evaluation were excluded. Six patients and two HC were further excluded based on the result of MRI preprocessing (see the method for details). This process left ninety-six schizophrenia patients and 122 HC as a final sample of our study. Written informed consent was obtained from all subjects. The authors assert that all procedures contributing to this work comply with the ethical standards of the relevant national and institutional committees on human experimentation and with the Helsinki Declaration of 1975, as revised in 2008. All procedures involving human subjects/patients were approved by the Ethics Committee of the Clinical Hospital of Chengdu Brain Science Institute.

Data acquisition and image preprocessing

MRI data were obtained on a 3-T GE Discovery MR 750 scanner at the MRI Center of the University of Electronic Science and Technology of China. Functional scans were performed using a standard echo-planar imaging (EPI) pulse sequence with the following scan parameters: TR/TE = 2000 ms/30 ms, flip angle (FA) = 90° , matrix size = 64×64 , field of view (FOV) = $240 \times 240 \text{ mm}^2$, 35 interleaved slices and slice thickness = 4 mm (no gap). During this resting-state fMRI scanning, each participant was instructed to stay relaxed and close his/her eyes without falling asleep. Each scan lasted for 510 s per subject (255 volumes). T1-weighted anatomical data were acquired using a MPRAGE (MEMPR) sequence (scan parameters: TR/TE = 1900 ms/3.43 ms, $FA = 90^{\circ}$, matrix size = 256×256 , FOV = $240 \text{ mm} \times 240 \text{ mm}$, slice thickness = 1 mm, voxel size = $0.9375 \text{ mm} \times 0.9375 \text{ mm} \times 1 \text{ mm}$, 160 slices). In both scans, foam pads were used to reduce head movement and scanner noise. The anatomical data were used to normalize functional data.

All preprocessing steps were carried out using the Data Processing & Analysis for (Resting-State) Brain Imaging

(DPABI v4.1(Yan, Wang, Zuo, & Zang, 2016), and Matlab scripts. Consistent with our previous study (Dong et al., 2018, 2020), functional images were (1) discarded in the first five volumes, (2) slice-time corrected, (3) realigned, (4) co-registered to the high-resolution 3D anatomic volume, (5) warped into MNI152 standard space (resampling the voxel size into 3×3×3 mm³), (6) underwent wavelet despiking of head motion artifacts(Patel et al., 2014)), (7) underwent regression of motion and non-relevant signals, including linear trend, Friston 24 head motion parameters (Friston, Williams, Howard, & Frackowiak, 1996; Satterthwaite et al., 2013) white matter (CompCor, 5 principal components), and CSF signal (CompCor, 5 principal components(Behzadi, Restom, Liau, & Liu, 2007)), and (8) were filtered using a band-pass filter (0.01-0.1 Hz). We excluded participants due to maximum head motion exceeding 2.5 mm or 2.5° rotation or with >10% frame-to-frame motion quantified by framewise displacements (FD>0.5mm (Power, Barnes, Snyder, Schlaggar, & Petersen, 2012))) during MRI acquisition. Besides, mean FD was evaluated in the two groups (Power et al. 2012). The mean FD for each participant was evaluated using the following formula:

$$FD = \frac{1}{M-1} \sum_{i=2}^{M} \sqrt{|\Delta d_{x_i^1}|^2 + |\Delta d_{y_i^1}|^2 + |\Delta d_{z_i^1}|^2 + |\Delta d_{x_i^2}|^2 + |\Delta d_{y_i^2}|^2 + |\Delta d_{z_i^2}|^2}$$

where M is the number of the fMRI time points, and $x_i^1/x_i^2, y_i^1/y_i^2$ and z_i^1/z_i^2 are translations/rotations at the *i*thtime point in the x,y and z directions, respectively; $\Delta d_{x_i^1=x_i^1-x_{i-1}^1}$. The global mean signal was not regressed out because this may distort between-group comparisons of inter-regional correlation (Saad et al., 2012). Besides, studies suggest that altered global signal is an important neuroimaging feature in schizophrenia (Hahamy et al., 2014; Yang et al., 2014).

Connectivity gradient analyses

Gradient mapping techniques describe a continuous coordinate system at the systems level that place sensory and motor networks on one end and transmodel network on the other. This approach thus provides us a simplified representation in terms of main dimensions to characterize the alteration of the macroscale cortical hierarchy in schizophrenia.

Specifically, the voxel-level connectivity matrix for each subject was computed using Fisher Z-transformed Pearson correlations. Based on previous studies (Dong et al., 2020; Guell, Schmahmann, Gabrieli, & Ghosh, 2018; Hong et al., 2019; Margulies et al., 2016; Vos De Wael et al., 2018), we thresholded the rsFC matrix with the top 10% of connections per row retained, whereas all others were zeroed. The negative connections were zeroed as well. Then, we used cosine distance to generate a similarity matrix that reflected the similarity of connectivity profiles between each pair of voxels. We used diffusion map embedding (Coifman et al., 2005), a nonlinear dimensionality reduction

algorithm, to identify a low-dimensional embedding from a high-dimensional connectivity matrix. This methodological strategy has been proved to successfully identify relevant aspects of functional organization in the cerebral cortex in previous studies (Hong et al., 2019; Margulies et al., 2016). Similar to Principal Component Analysis (PCA), diffusion map embedding can identify principal gradient components accounting for the variance in descending order. The result of diffusion embedding is not one single mosaic of discrete networks, but multiple, continuous maps (gradients), which capture the similarity of each voxel's functional connections along with a continuous space. All gradients are orthogonal to each other and capture a portion of data variability in descending order.

There is a single parameter α to control how the density of sampling points affects the underlying manifold ($\alpha=0$, the maximal influence of sampling density; $\alpha=1$, no influence of sampling density) in the diffusion map embedding algorithm. Following previous studies (Guell et al., 2018; Hong et al., 2019; Margulies et al., 2016), we set $\alpha=0.5$, which can help retain the global relations between data points in the embedded space. To compare between the SZ and HC groups, we used an average connectivity matrix calculated from all patients and controls to produce a group-level gradient component template. We then performed Procrustes rotation to align the gradients of each participant to this template, following the strategy of previous analyses (Langs, Golland, & Ghosh, 2015). To maximize interpretability, we only used the first gradient component in our analyses. The first gradient explains as much of the variance in the data as possible (Figure S1) and, from a neurobiological point of view, represents a well-understood sensorimotor-to-transmodal organizational principle in the cerebral cortex connections.

Stepwise functional connectivity analyses

SFC analysis is a graph-theory-based method that detects both direct and indirect functional couplings from a defined seed region to other regions in the brain. More importantly, SFC analytical approach allows for analysis of indirect FC (medium and large connectivity distances from the seed), which is thought to provide information integration about hierarchical flow across specific brain networks (Sepulcre, 2014; Sepulcre, Sabuncu, Yeo, Liu, & Johnson, 2012). This approach thus enables us to investigate the presence of atypical functional transitions from unimodal to multimodal cortical areas within the framework of the cortical hierarchy in schizophrenia.

SFC analysis computes the number of functional paths between defined seed regions and every other voxel in the brain at successive numbers of relay stations or "link-step" distances (Sepulcre, 2014; Sepulcre et al., 2012). Hence, it complements connectivity gradient approaches by allowing voxel-level functional connections to be assessed at a range of intermediate relay stations. Following previous studies (Martínez et al., 2019; Sepulcre et al., 2012), connectivity matrices were first filtered to include only positive correlations due to the ambiguous interpretation of

negative correlations. After that, the connectivity matrices were further filtered to contain only correlations surviving a stringent false discovery rate (FDR) correction (q < 0.001). Finally, we submitted the resulting FDR thresholded matrices to SFC analysis.

Given that deficits of visual, auditory, and somatosensory processing in schizophrenia were consistently observed (for reviews (Javitt, 2009; Javitt & Freedman, 2015)), three bilateral primary sensory seed regions of interest (ROIs) including visual (MNI coordinate x, y, z: -14/10 [left/right], -78, 8; (Brodmann 17, V1)), auditory (-54/58, -14, 8; (Brodmann 22, A1)) and somatosensory (-42/38, -29, 65; (Brodmann 3, hand area)) areas (Sepulcre et al., 2012), were defined as cubic regions of eight voxels each. To assess the degree of combined SFC of all sensory seeds irrespective of modality, a combined mask was constructed by combining information from all three primary sensory regions. The method is described in detail elsewhere (Sepulcre, 2014; Sepulcre et al., 2012) and schematically represented in Figure 1D.

The degree of SFC of a given voxel of the brain is defined as the number of functional paths connecting that voxel with an a priori selected seed region at a specific link-step distance. A link-step distance is defined as the number of edges that pertain to a path connecting a given voxel to the seed regions. At each link step, SFC maps were standardized to Z-scores by subtracting the mean and dividing by its standard deviation (SD) to yield SFC values. Therefore, each SFC map represents a relative increase of connectivity degree across different link-step distances. As demonstrated in previous studies (Buckner et al., 2009; Sepulcre et al., 2012), functional pathways "collapse" into the cortical hubs of the adult human brain after link-step distances >7; accordingly, we constrained our SFC analysis to seven link-step distances.

Statistical and Control Analyses

To visualize the gradient pattern, group mean maps were calculated for each group. One-sample t-tests were performed to characterize the SFC patterns at each of the seven link-step distances in the HC and schizophrenia groups separately (p<0.001 uncorrected, only for purposes of clear data visualization).

Three analyses were performed to ensure robustness of the main findings. First, because GSR is controversial, we repeated core analyses (gradient and SFC) with GSR. Second, as shown in Table 1, while there was no significant difference in mean framewise displacement (FD) between patients and controls, we also corrected for head motion in the subsequent statistical comparisons by using mean FD as covariate (Yan et al., 2013). And, to investigate the potential effects of micro head motion on our findings, we calculated Pearson Correlations between altered gradients, SFC value and mean FD. Third, to target the potentially confounding effect of medication, we calculated Pearson

Correlations between altered gradients, SFC value and medication measured by chlorpromazine equivalents.

Data and code availability

The preprocessing software is freely available (DPABI v4.1, http://rfmri.org/dpabi). The code for gradient analysis is openly available via the BrainSpace toolbox (http://brainspace.readthedocs.io) (Wael et al., 2020). The code for SFC analysis is available via a direct request to Jorge Sepulcre. Results were visualized with BrainNet Viewer v1.7 (https://www.nitrc.org/projects/bnv/) (Xia, Wang, & He, 2013). The imaging and clinical data are made available via a direct request to the corresponding author (Cheng Luo). Sharing and re-use of imaging and clinical data need the expressed written permission of the authors and clearance from the relevant institutional review boards.

Supplementary results

Global signal regression

Given recent studies found evidence of altered global signal in schizophrenia patients, supporting the idea that the global signal contains pathophysiologically relevant information, we did not performed global signal regression (GSR) in our main text. However, currently there is no consensus in the neuroimaging field whether to do GSR when computing functional connectivity. To investigate the potential effects of GSR on our findings, we repeated core analyses (gradient and SFC) with GSR, which does not significantly affect the trends of overall results (Figure S2-3), although increased SFC degree was found between unimodal seeds and frontoparietal regions, i.e., middle / superior frontal gyrus, inferior parietal lobule, supramarginal gyrus, and dorsal precuneus), and ventral attention regions (dorsal anterior cingulate cortex and bilateral anterior insular cortex / central opercular cortex) at all link-step distances (Step1 to 7). These differences were only found at early and medium link-step distances (Step1 to 4) without conducting GSR. Overall, the relatively consistent results with and without GSR could indicate the observed main findings reflected the reliable pathophysiologic mechanism of schizophrenia.

Control analyses

We summarize three analyses that ensured robustness of results. GSR did not significantly affect trends of overall results (gradient and SFC analyses).. The relatively consistent results between without GSR and with GSR indicated the observed main findings reflected the reliable pathophysiology of schizophrenia. Second, we found that FD was not associated with altered gradient and SFC degree scores (all p values in this analysis were larger than 0.05), indicating that group differences reported here are rather unlikely to be driven by head motion. Similarly, Chlorpromazine equivalents were not associated with an altered gradient and SFC degree (all p >0.1), suggesting that these changes are unlikely to be mainly driven by medication.

- Behzadi, Y., Restom, K., Liau, J., & Liu, T. T. (2007). A component based noise correction method (CompCor) for BOLD and perfusion based fMRI. *NeuroImage*, *37*(1), 90–101. https://doi.org/10.1016/j.neuroimage.2007.04.042
- Buckner, R. L., Sepulcre, J., Talukdar, T., Krienen, F. M., Liu, H., Hedden, T., ... Johnson, K. A. (2009). Cortical hubs revealed by intrinsic functional connectivity: Mapping, assessment of stability, and relation to Alzheimer's disease. *Journal of Neuroscience*, *29*(6), 1860–1873. https://doi.org/10.1523/JNEUROSCI.5062-08.2009
- Coifman, R. R., Lafon, S., Lee, A. B., Maggioni, M., Nadler, B., Warner, F., & Zucker, S. W. (2005). Geometric diffusions as a tool for harmonic analysis and structure definition of data: Multiscale methods. *Proceedings of the National Academy of Sciences of the United States of America*, 102(21), 7432–7437.
- Dong, D., Duan, M., Wang, Y., Zhang, X., Jia, X., Li, Y., ... Luo, C. (2018). Reconfiguration of Dynamic Functional Connectivity in Sensory and Perceptual System in Schizophrenia. *Cerebral Cortex*, 1–13. https://doi.org/10.1093/cercor/bhy232
- Dong, D., Luo, C., Guell, X., Wang, Y., He, H., Duan, M., & Eickhoff, S. B. (2020). Compression of Cerebellar Functional Gradients in Schizophrenia Debo. *Schizophrenia Bulletin*, 1–14. https://doi.org/10.1093/schbul/sbaa016
- Friston, K. J., Williams, S., Howard, R., & Frackowiak, R. S. J. (1996). Movement Related Effects In FMRI. *Magnetic Resonance in Medicine*, *3*(35), 346–355.
- Guell, X., Schmahmann, J. D., Gabrieli, J. DE, & Ghosh, S. S. (2018). Functional gradients of the cerebellum. *ELife*, 7, 1–22. https://doi.org/10.7554/elife.36652
- Hahamy, A., Calhoun, V., Pearlson, G., Harel, M., Stern, N., Attar, F., ... Salomon, R. (2014). Save the Global: Global Signal Connectivity as a Tool for Studying Clinical Populations with Functional Magnetic Resonance Imaging. *Brain Connectivity*, 4(6), 395–403. https://doi.org/10.1089/brain.2014.0244
- Hong, S. J., de Wael, R. V., Bethlehem, R. A. I., Lariviere, S., Paquola, C., Valk, S. L., ... Bernhardt, B. C. (2019). Atypical functional connectome hierarchy in autism. *Nature Communications*, *10*(1), 1–13. https://doi.org/10.1038/s41467-019-08944-1
- Javitt, D. C. (2009). Sensory processing in schizophrenia: Neither simple nor intact. *Schizophrenia Bulletin*, *35*(6), 1059–1064. https://doi.org/10.1093/schbul/sbp110
- Javitt, D. C., & Freedman, R. (2015). Sensory processing dysfunction in the personal experience and neuronal machinery of schizophrenia. *American Journal of Psychiatry*, *172*(1), 17–31. https://doi.org/10.1176/appi.ajp.2014.13121691
- Langs, G., Golland, P., & Ghosh, S. S. (2015). Predicting Activation Across Individuals with Resting-State Functional Connectivity

 Based Multi-Atlas Label Fusion. *Med Image Comput Comput Assist Interv.*, 313–320.

 https://doi.org/10.1007/978-3-319-24571-3 38
- Margulies, D. S., Ghosh, S. S., Goulas, A., Falkiewicz, M., Huntenburg, J. M., Langs, G., ... Smallwood, J. (2016). Situating the default-mode network along a principal gradient of macroscale cortical organization. *Proceedings of the National Academy of Sciences*, *113*(44), 12574–12579. https://doi.org/10.1073/pnas.1608282113
- Martínez, K., Martínez-garcía, M., Marcos-vidal, L., Janssen, J., Castellanos, F. X., Pretus, C., ... Carmona, S. (2019).

 Sensory-to-Cognitive Systems Integration Is Associated With Clinical Severity in Autism Spectrum Disorder. *Journal of the American Academy of Child & Adolescent Psychiatry*. https://doi.org/10.1016/j.jaac.2019.05.033
- Patel, A. X., Kundu, P., Rubinov, M., Jones, P. S., Vértes, P. E., Ersche, K. D., ... Bullmore, E. T. (2014). A wavelet method for modeling and despiking motion artifacts from resting-state fMRI time series. *NeuroImage*, *95*, 287–304. https://doi.org/10.1016/j.neuroimage.2014.03.012
- Power, J. D., Barnes, K. A., Snyder, A. Z., Schlaggar, B. L., & Petersen, S. E. (2012). Spurious but systematic correlations in functional connectivity MRI networks arise from subject motion. *NeuroImage*, *59*(3), 2142–2154. https://doi.org/10.1016/j.neuroimage.2011.10.018
- Saad, Z. S., Gotts, S. J., Murphy, K., Chen, G., jo, H. J., Martin, A., & Cox, R. W. (2012). Trouble at Rest: How Correlation Patterns and Group Differences Become Distorted After Global Signal Regression. *Brain Connectivity*, *2*(1), 25–32. https://doi.org/10.1089/brain.2012.0080
- Satterthwaite, T. D., Elliott, M. A., Gerraty, R. T., Ruparel, K., Loughead, J., Calkins, M. E., ... Wolf, D. H. (2013). An improved framework for confound regression and filtering for control of motion artifact in the preprocessing of resting-state functional connectivity data. *NeuroImage*, 64(1), 240–256. https://doi.org/10.1016/j.neuroimage.2012.08.052
- Sepulcre, J. (2014). Functional streams and cortical integration in the human brain. *Neuroscientist*, 20(5), 499–508.

- https://doi.org/10.1177/1073858414531657
- Sepulcre, J., Sabuncu, M. R., Yeo, T. B., Liu, H., & Johnson, K. A. (2012). Stepwise connectivity of the modal cortex reveals the multimodal organization of the human brain. *Journal of Neuroscience*, *32*(31), 10649–10661. https://doi.org/10.1523/JNEUROSCI.0759-12.2012
- Vos De Wael, R., Larivière, S., Caldairou, B., Hong, S. J., Margulies, D. S., Jefferies, E., ... Bernhardt, B. C. (2018). Anatomical and microstructural determinants of hippocampal subfield functional connectome embedding. *Proceedings of the National Academy of Sciences of the United States of America*, 115(40), 10154–10159. https://doi.org/10.1073/pnas.1803667115
- Wael, R. V. de, Benkarim, O., Paquola, C., Lariviere, S., Royer, J., Tavakol, S., ... Bernhardt, B. C. (2020). BrainSpace: a toolbox for the analysis of macroscale gradients in neuroimaging and connectomics datasets. *Communications Biology*, *3*, 1–10.
- Xia, M., Wang, J., & He, Y. (2013). BrainNet Viewer: A Network Visualization Tool for Human Brain Connectomics. *PLoS ONE*, *8*(7). https://doi.org/10.1371/journal.pone.0068910
- Yan, C. G., Cheung, B., Kelly, C., Colcombe, S., Craddock, R. C., Di Martino, A., ... Milham, M. P. (2013). A comprehensive assessment of regional variation in the impact of head micromovements on functional connectomics. *NeuroImage*, *76*, 183–201. https://doi.org/10.1016/j.neuroimage.2013.03.004
- Yan, C. G., Wang, X. Di, Zuo, X. N., & Zang, Y. F. (2016). DPABI: Data Processing & Analysis for (Resting-State) Brain Imaging. Neuroinformatics, 14(3), 339–351. https://doi.org/10.1007/s12021-016-9299-4
- Yang, G. J., Murray, J. D., Repovs, G., Cole, M. W., Savic, A., Glasser, M. F., ... Anticevic, A. (2014). Altered global brain signal in schizophrenia. *Proceedings of the National Academy of Sciences of the United States of America*, 111(20), 7438–7443. https://doi.org/10.1073/pnas.1405289111
- Yeo, B. T., Krienen, F. M., Sepulcre, J., Sabuncu, M. R., Lashkari, D., Hollinshead, M., . . . Polimeni, J. R. (2011). The organization of the human cerebral cortex estimated by intrinsic functional connectivity. *Journal of neurophysiology, 106*(3), 1125-1165 doi:10.1152/jn.00338.2011

Table S1. Group differences in degree of stepwise functional connectivity

| Brain regions | T value | Voxels (k) | MNI coordinates | | | |
|---|---------|------------|-----------------|-----|-----|--|
| _ | | - | X | Y | Z | |
| One step | | | | | | |
| Patients>Controls | | | | | | |
| L Inferior Temporal Gyrus | 3.90 | 23 | -42 | -54 | -12 | |
| L Angular Gyrus / Supramarginal Gyrus | 4.38 | 49 | -43 | -55 | 55 | |
| / Inferior Parietal Lobule | | | | | | |
| L Middle Frontal Gyrus | 4.50 | 47 | -36 | 42 | 30 | |
| L Superior Frontal Gyrus | 4.92 | 70 | -18 | 12 | 66 | |
| Anterior Cingulate Cortex / | 5.14 | 62 | 0 | 30 | 24 | |
| Supp_Motor_Area | | | | | | |
| R Middle Frontal Gyrus | 5.17 | 43 | 36 | 36 | 36 | |
| L Precuneus Cortex | 5.38 | 50 | -6 | -72 | 54 | |
| R Supramarginal Gyrus /Angular Gyrus / Inferior Parietal Lobule | 5.95 | 71 | 54 | -36 | 18 | |
| R Insular Cortex / Central Opercular | 6.21 | 61 | 48 | 12 | -6 | |
| Cortex / Superior Temporal Gyrus | | | | | | |
| L Temporal Pole / Insular Cortex / | 6.35 | 73 | -48 | 6 | -6 | |
| Central Opercular Cortex / Superior | | | | | | |
| Temporal Gyrus | | | | | | |
| Patients< Controls | | | | | | |
| R pre/postcentral Gyrus | -7.61 | 200 | 48 | -18 | 42 | |
| L pre/postcentral Gyrus | -6.56 | 92 | -54 | -18 | 36 | |
| Bilateral Calcarine / Lingual Gyrus / | -5.04 | 203 | 6 | -66 | 12 | |
| Cuneus | | | | | | |
| Two steps | | | | | | |
| Patients>Controls | | | | | | |
| L Middle Frontal Gyrus | 4.51 | 55 | -36 | 42 | 30 | |
| R Middle Frontal Gyrus | 5.18 | 57 | 36 | 36 | 36 | |
| L Supramarginal Gyrus / Inferior | 5.48 | 89 | -66 | -48 | 18 | |
| Parietal Lobule / Angular Gyrus / | | | | | | |
| L Superior Frontal Gyrus / Anterior | 5.60 | 156 | -18 | 12 | 66 | |
| Cingulate Cortex / Supp_Motor_Area | T - C 2 | | 40 | 10 | 0 | |
| R Insular Cortex / Central Opercular | 5.62 | 68 | 48 | 12 | 0 | |
| Cortex / Superior Temporal Gyrus / | | | | | | |
| Inferior Frontal Gyrus | 5.00 | 106 | ~ 4 | 26 | 1.0 | |
| R Angular Gyrus / Supramarginal Gyrus | 5.92 | 106 | 54 | -36 | 18 | |
| / Inferior Parietal Lobule | c 10 | 1.40 | | | | |
| R / L Precuneus Cortex | 6.12 | 148 | 6 | -66 | 66 | |
| L Temporal Pole / Insular Cortex / | 6.63 | 80 | -48 | 6 | -6 | |
| Central Opercular Cortex / Superior | | | | | | |
| Temporal Gyrus / Inferior Frontal Gyrus | | | | | | |
| Patients < Controls | 7.70 | 260 | 40 | 10 | 40 | |
| R pre/postcentral Gyrus | -7.78 | 260 | 48 | -18 | 42 | |
| L pre/postcentral Gyrus | -6.62 | 121 | -54 | -18 | 36 | |
| Bilateral Middle Occipital Gyrus / | -5.01 | 424 | 42 | -66 | 0 | |
| Calcarine / Lingual Gyrus / Cuneus | | | | | | |

Three steps

| Patients>Controls | | | | | |
|---|-------|-----|-----|-----|-----|
| L Supramarginal Gyrus / Angular Gyrus | 4.38 | 80 | -66 | -48 | 18 |
| / Inferior Parietal Lobule | | | | | |
| L Middle Frontal Gyrus | 4.75 | 63 | -36 | 24 | 36 |
| Middle / Inferior Temporal Gyrus / | 5.22 | 84 | 54 | -24 | -18 |
| Insular Cortex /Central Opercular | | | | | |
| Cortex | | | | | |
| R Middle Frontal Gyrus | 5.26 | 67 | 36 | 30 | 36 |
| R Angular Gyrus / Supramarginal Gyrus | 5.72 | 96 | 48 | -48 | 36 |
| / Inferior Parietal Lobule | | | | | |
| L Superior Frontal Gyrus / Anterior | 5.74 | 162 | -12 | 18 | 60 |
| Cingulate Cortex / Supp_Motor_Area | | | | | |
| R/L Precuneus Cortex / Middle | 6.07 | 124 | 0 | -54 | 72 |
| Cingulum Cortex | | | | | |
| Insular Cortex / Central Opercular | 6.45 | 90 | -48 | 12 | -6 |
| Cortex / Temporal Pole / Middle | | | | | |
| Temporal Gyrus / Inferior Frontal Gyrus | | | | | |
| Patients< Controls | | | | | |
| R pre/postcentral Gyrus | -7.43 | 240 | 48 | -18 | 42 |
| L pre/postcentral Gyrus | -6.46 | 190 | -54 | -18 | 36 |
| Bilateral Middle Occipital Gyrus / | -5.84 | 537 | 42 | -66 | 0 |
| Calcarine / Lingual Gyrus / Cuneus | | | | | |
| Four steps | | | | | |
| Patients>Controls | | | | | |
| Middle Cingulum Gyrus | 4.00 | 21 | 0 | -18 | 30 |
| L Middle Frontal Gyrus | 4.27 | 50 | -36 | 12 | 36 |
| R Middle Frontal Gyrus | 4.46 | 53 | 36 | 30 | 36 |
| R Inferior Parietal Lobule / | 4.47 | 43 | 42 | -48 | 36 |
| Supramarginal Gyrus /Angular Gyrus | | | | | |
| L Supramarginal Gyrus / Inferior | 5.13 | 45 | -66 | -48 | 18 |
| Parietal Lobule / Angular Gyrus | | | | | |
| Anterior Cingulate Cortex / Superior | 5.14 | 113 | -5 | 11 | 58 |
| Frontal Gyrus / Inferior Frontal Gyrus | | | | | |
| Inferior / Middle temporal Gyrus / | 5.42 | 178 | 42 | -6 | -30 |
| Inferior Frontal Gyrus | | | | | |
| Inferior / Middle temporal Gyrus / | 5.52 | 272 | -46 | -13 | -25 |
| Inferior Frontal Gyrus | | | | | |
| L Insular Cortex/ Central Opercular | 6.04 | 37 | -48 | 12 | -6 |
| Cortex | | | | | |
| Patients< Controls | | | | | |
| R pre/postcentral Gyrus | -6.84 | 256 | 54 | -12 | 42 |
| L pre/postcentral Gyrus | -6.04 | 170 | -54 | -18 | 36 |
| Bilateral Middle Occipital Gyrus / | -5.83 | 546 | 42 | -66 | 0 |
| Calcarine / Lingual Gyrus / Cuneus | | | | | |
| Five steps | | | | | |
| Patients>Controls | | | | | |
| Middle Temporal Gyrus | 4.26 | 20 | 54 | -30 | -12 |
| L Superior Frontal Gyrus / | 4.93 | 158 | -6 | 12 | 60 |
| Supp_Motor_Area | | | | | |
| | | | | | |

| L Middle / Inferior Temporal Gyrus / | 5.19 | 215 | -42 | 6 | -30 |
|---|-------|-----|-----|-----|-----|
| Temporal_Pole / Inferior Frontal Gyrus | | | | | |
| Middle / Inferior Temporal Gyrus / | 5.27 | 101 | 42 | 0 | -36 |
| Inferior Frontal Gyrus | | | | | |
| Patients< Controls | | | | | |
| R pre/postcentral Gyrus | -6.21 | 209 | 54 | -12 | 42 |
| L pre/postcentral Gyrus | -5.95 | 92 | -36 | -30 | 60 |
| Bilateral Middle Occipital Gyrus / | -5.53 | 545 | 42 | -66 | 0 |
| Calcarine / Lingual Gyrus / Cuneus | | | | | |
| Six steps | | | | | |
| Patients>Controls | | | | | |
| L Frontal_Sup_Orb | 4.03 | 42 | -18 | 60 | -6 |
| L Superior Frontal Gyrus / | 4.51 | 84 | -6 | 12 | 60 |
| Supp_Motor_Area | | | | | |
| R Middle Temporal Gyrus | 4.84 | 29 | 60 | -36 | -6 |
| L Middle / Inferior Temporal Gyrus | 5.60 | 212 | -42 | 6 | -30 |
| /Temporal_Pole / Inferior Frontal Gyrus | | | | | |
| R Middle / Inferior Temporal Gyrus / | 5.65 | 109 | 42 | 0 | -36 |
| Temporal_Pole | | | | | |
| Patients< Controls | | | | | |
| R pre/postcentral Gyrus | -5.92 | 227 | 48 | -18 | 42 |
| L pre/postcentral Gyrus | -5.50 | 180 | -36 | -30 | 60 |
| Bilateral Middle Occipital Gyrus / | -5.26 | 512 | 42 | -66 | 0 |
| Calcarine / Lingual Gyrus / Cuneus | | | | | |
| Seven steps | | | | | |
| Patients>Controls | | | | | |
| L Middle Frontal Gyrus | 3.44 | 22 | -24 | 54 | 18 |
| Superior-Medial Frontal Gyrus | 4.25 | 21 | 0 | 42 | 42 |
| L Superior Frontal Gyrus / | 4.27 | 42 | -6 | 12 | 60 |
| Supp_Motor_Area | | | | | |
| R Middle Temporal Gyrus | 4.84 | 31 | 60 | -36 | -6 |
| R Middle / Inferior Temporal Gyrus | 5.78 | 119 | 42 | 0 | -36 |
| /Temporal_Pole | | | | | |
| L Middle / Inferior Temporal Gyrus / | 5.92 | 220 | -42 | 6 | -30 |
| Temporal_Pole / Inferior Frontal Gyrus | | | | | |
| Patients< Controls | | | | | |
| R pre/postcentral Gyrus | -5.77 | 200 | 48 | -18 | 42 |
| L pre/postcentral Gyrus | -5.27 | 196 | -36 | -30 | 60 |
| Bilateral Middle Occipital Gyrus / | -5.26 | 486 | 42 | -66 | 0 |
| Calcarine / Lingual Gyrus / Cuneus | | | | | |

Notes: L, left side of brain; R, right side of brain. Results are reported using a voxel-wise FDR threshold of P < .05 and an additional cluster-size threshold of k=20.

Table S2. Association Between Atypical Gradient, SFC Degree and Clinical Severity in Schizophrenia

| Index | Regions | PANSS-P | | PANSS-N | | PANSS-G | | PANSS-T | |
|-----------|--|---|-------|---------|-------|---------|-------|---------|-------|
| | | r | р | r | p | r | p | r | p |
| Gradient | Ventral Medial Frontal Gyrus | -0.032 | 0.799 | -0.318* | 0.010 | -0.031 | 0.810 | -0.173 | 0.172 |
| Gradient | L Anterior Insula | -0.007 | 0.953 | -0.258 | 0.039 | 0.092 | 0.470 | -0.155 | 0.222 |
| Gradient | L Precuneus | -0.366* | 0.002 | -0.102 | 0.423 | -0.183 | 0.147 | -0.292 | 0.019 |
| SFC-step1 | L Superior Frontal Gyrus | -0.085 | 0.499 | -0.051 | 0.688 | -0.278 | 0.026 | -0.184 | 0.144 |
| | R Anterior Insular Cortex / | -0.290 | 0.020 | -0.178 | 0.157 | -0.303 | 0.014 | -0.345* | 0.005 |
| | Central Opercular Cortex | | | | | | | | |
| | L Anterior Insular Cortex / | -0.354* | 0.004 | -0.221 | 0.078 | -0.259 | 0.038 | -0.374* | 0.002 |
| | Central Opercular Cortex | | | | | | | | |
| | R pre/postcentral Gyrus | 0.250 | 0.046 | 0.090 | 0.476 | 0.353* | 0.004 | 0.309 | 0.012 |
| | L pre/postcentral Gyrus | 0.186 | 0.139 | 0.152 | 0.227 | 0.310 | 0.012 | 0.290 | 0.020 |
| | R Lingual Gyrus / Cuneus | 0.324* | 0.008 | -0.104 | 0.389 | -0.036 | 0.776 | 0.079 | 0.531 |
| SFC-step2 | L Anterior Insular Cortex / | -0.238 | 0.057 | -0.343* | 0.005 | -0.276 | 0.027 | -0.386* | 0.001 |
| | Central Opercular Cortex | | | | | | | | |
| | R pre/postcentral Gyrus | 0.243 | 0.052 | 0.163 | 0.197 | 0.379* | 0.002 | 0.351* | 0.004 |
| SFC-step3 | L Anterior Insular Cortex / | -0.159 | 0.208 | -0.383* | 0.001 | -0.252 | 0.044 | -0.358* | 0.003 |
| | Central Opercular Cortex | | | | | | | | |
| | R pre/postcentral Gyrus | 0.164 | 0.194 | 0.166 | 0.190 | 0.326* | 0.008 | 0.293 | 0.018 |
| | R Middle Occipital Gyrus / | 0.166 | 0.190 | 0.299 | 0.016 | 0.026 | 0.833 | -0.050 | 0.693 |
| | Lingual Gyrus / Cuneus | | | | | | | | |
| SFC-step4 | L Middle Frontal Gyrus | 0.050 | 0.689 | 0.334* | 0.006 | 0.102 | 0.418 | 0.220 | 0.079 |
| | L Anterior Insular Cortex / | -0.025 | 0.839 | -0.369* | 0.002 | -0.226 | 0.072 | -0.280 | 0.024 |
| | Central Opercular Cortex | | | | | | | | |
| | R Middle Occipital Gyrus / | 0.163 | 0.198 | 0.293 | 0.018 | 0.015 | 0.904 | -0.054 | 0.671 |
| | Lingual Gyrus / Cuneus | | | | | | | | |
| SFC-step5 | L pre/postcentral Gyrus | 0.029 | 0.816 | 0.324* | 0.008 | 0.247 | 0.048 | 0.270 | 0.030 |
| | R Middle Occipital Gyrus / | 0.109 | 0.389 | 0.247 | 0.049 | -0.024 | 0.850 | -0.074 | 0.559 |
| | Lingual Gyrus / Cuneus | | | | | | | | |
| SFC-step6 | R pre/postcentral Gyrus | 0.049 | 0.696 | 0.170 | 0.177 | 0.262 | 0.036 | 0.215 | 0.086 |
| | L pre/postcentral Gyrus | 0.010 | 0.933 | 0.313 | 0.011 | 0.255 | 0.041 | 0.260 | 0.037 |
| | R Middle Occipital Gyrus / | 0.066 | 0.601 | 0.259 | 0.038 | -0.069 | 0.587 | -0.118 | 0.349 |
| | Lingual Gyrus / Cuneus | | | | | | | | |
| SFC-step6 | R pre/postcentral Gyrus | 0.039 | 0.753 | 0.169 | 0.181 | 0.255 | 0.041 | 0.207 | 0.09 |
| | L pre/postcentral Gyrus | 0.006 | 0.961 | 0.307 | 0.013 | 0.256 | 0.041 | 0.256 | 0.041 |
| | R Middle Occipital Gyrus / | 0.057 | 0.648 | 0.264 | 0.035 | -0.073 | 0.538 | -0.128 | 0.309 |
| | Lingual Gyrus / Cuneus | | | | | | | | |
| | SZ>HC | The higher value is lined to the worse clinical symptoms | | | | | | | |
| | SZ <hc< td=""><td colspan="7">The higher value is lined to the better clinical symptoms</td></hc<> | The higher value is lined to the better clinical symptoms | | | | | | | |

Notes: L, left side of brain; R, right side of brain; * FDR p<0.05 corrected. PANSS-P, PANSS-Positive Symptoms; PANSS-N, PANSS-Negative Symptoms; PANSS-G, PANSS-General Symptoms; PANSS-T, PANSS-Total Symptoms. Note that higher scores in PANSS indicate increased severity of symptoms.

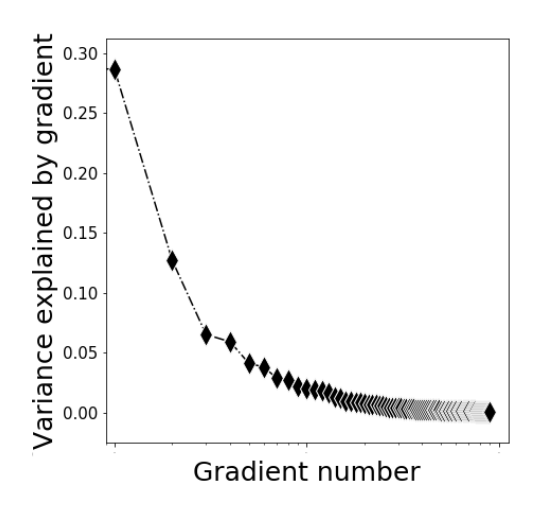


Figure S1. Variance explained by gradient.

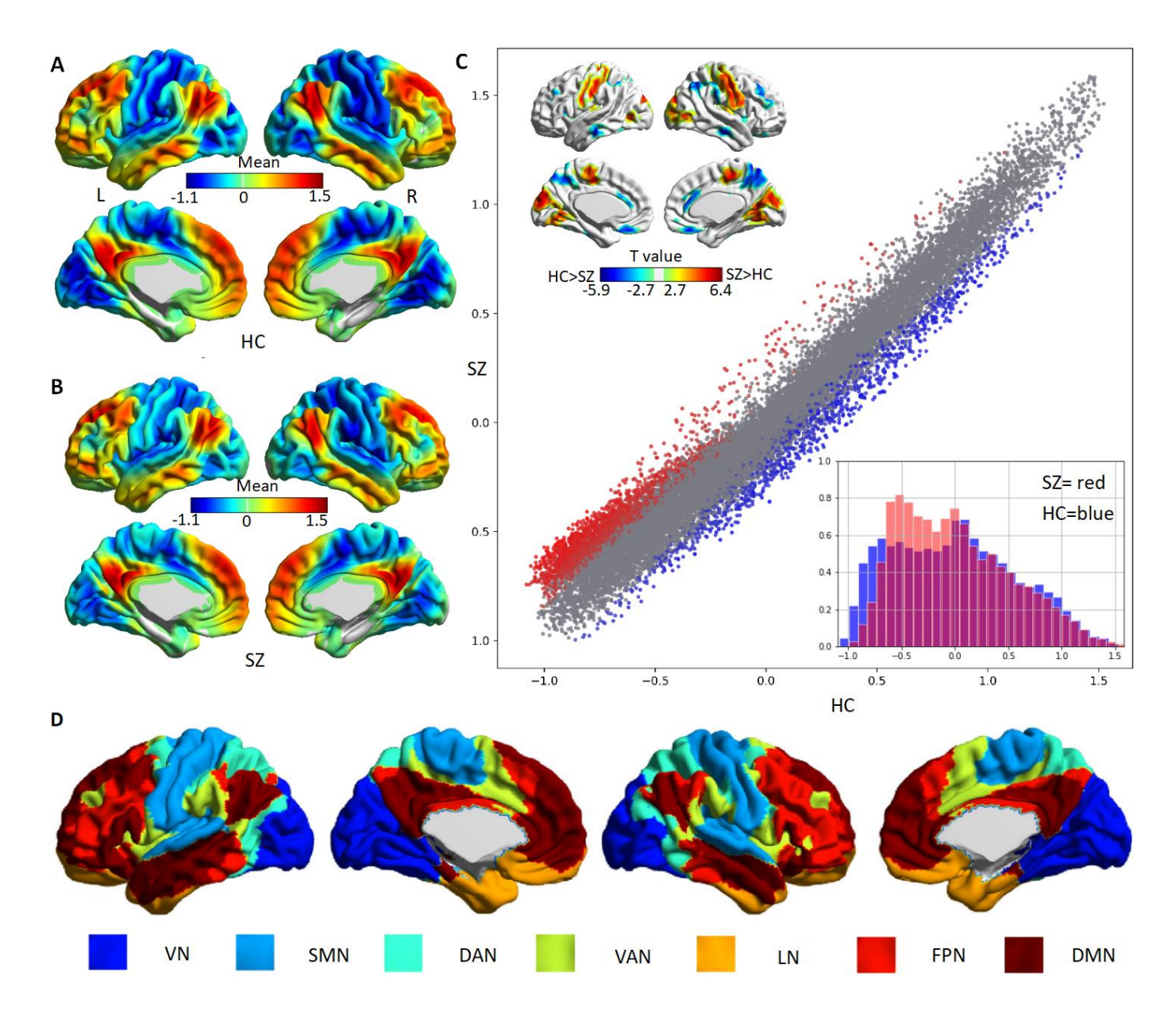


Figure S2. Group mean patterns and statistical differences in the cerebral principal functional gradient with GSR. (A) Mean gradient pattern in HC. (B) Mean gradient pattern in SZ. (C) Significant group differences between SZ and HC. Scatterplot represents cerebral gradient of SZ (y axis) vs. cerebral gradient of HC (x axis). Scatterplot colors correspond to group differences map as shown in top left corner of Figure S2(C): higher gradient value in SZ (red), and lower gradient value in SZ (blue) compared to HC. Compressed gradient pattern in SZ is shown in density histograms in bottom right corner of Figure S2(C). All results are shown after FDR correction (P < 0.05). (D) Yeo network classification (Yeo et al., 2011).

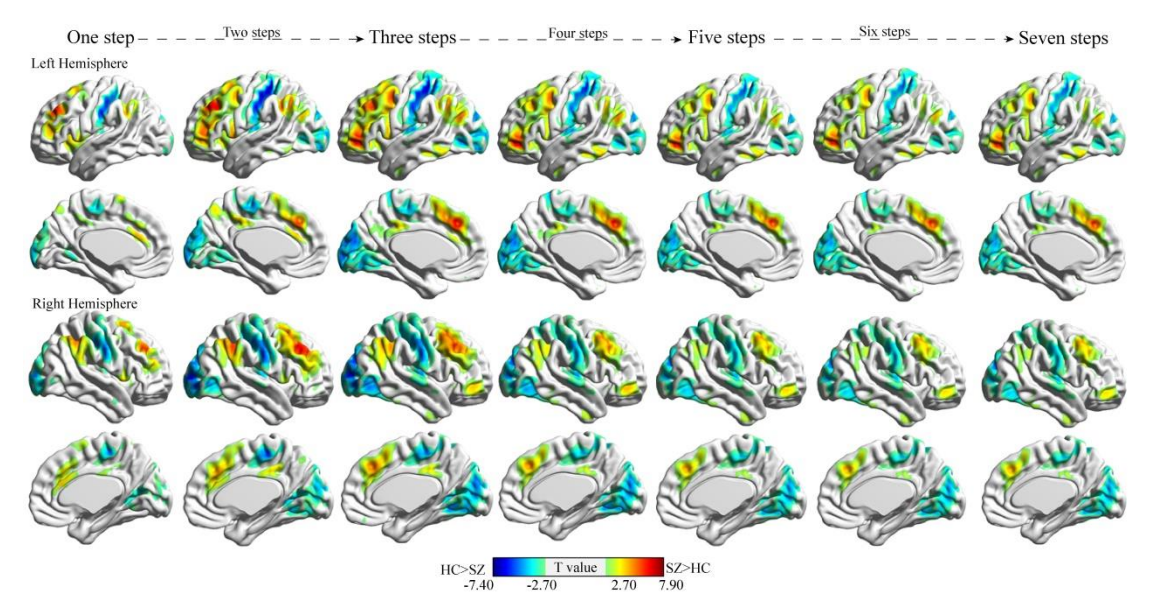


Figure S3. Group differences between schizophrenia (SZ) and healthy control (HC) in stepwise functional connectivity degree with GSR. All results are shown after FDR correction (P < 0.05).

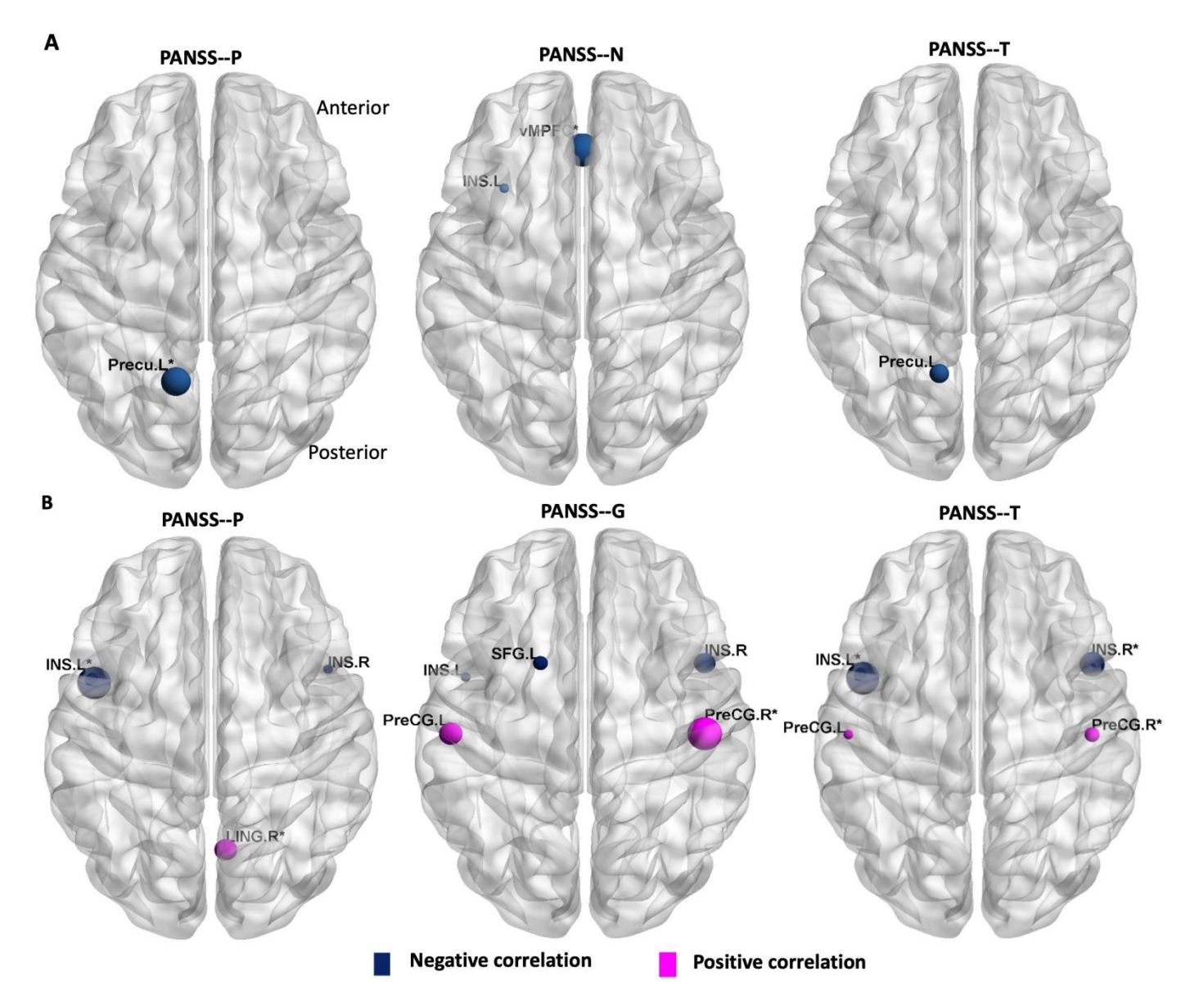


Figure S4. Correlations between altered functional gradient, SFC and clinical variables. (A) The correlation between altered functional gradient and clinical variables. (B) The correlation between altered SFC at one-link step distance. It should be noted that because the trends of correlation between clinical severity and altered SFC at each of the seven link-step distances were similar across the seven link-step distances. For clarity, we only showed the results at one-link step distance. PANSS-P, PANSS-positive symptoms scores; PANSS-N, PANSS-negative symptoms scores; PANSS-G, PANSS-general psychopathology symptoms scores; PANSS-T, PANSS-total symptoms scores; Precu.L, L precuneus; INS.R, R insular cortex; INS.L, L insular cortex; vMPFC, ventromedial prefrontal cortex; LING.R, R lingual gyrus; SFG.L, L superior frontal gyrus; PreCG.L, L precentral gyrus; PreCG.R, R precentral gyrus. Size of plots is weighted by r value. * represents significant correlation after FDR corrected (p < 0.05).

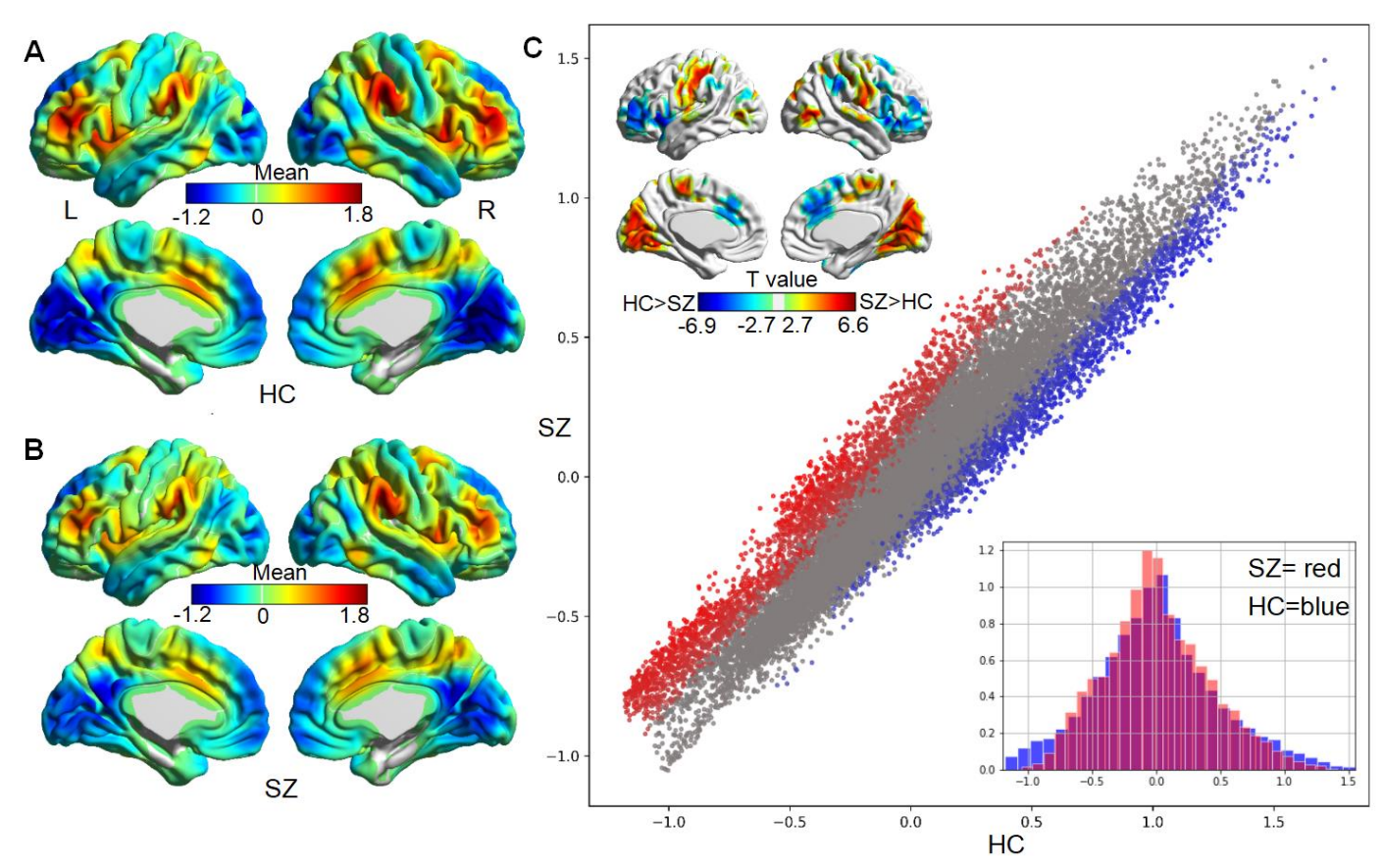


Figure S5. Group mean patterns and statistical differences in the cerebral second functional gradient. (A) Mean gradient pattern in HC. (B) Mean gradient pattern in SZ. (C) Significant group differences between SZ and HC. Scatterplot represents cerebral gradient of SZ (y axis) vs. cerebral gradient of HC (x axis). Scatterplot colors correspond to group differences map as shown in top left corner of Figure S5(C): higher gradient value in SZ (red), and lower gradient value in SZ (blue) compared to HC. Compressed gradient pattern in SZ is shown in density histograms in bottom right corner of Figure S5(C). All results are shown after FDR correction (P < 0.05).